Electromagnetic theory of enhanced Raman scattering by molecules adsorbed on rough surfaces

Joel Gersten

Department of Physics, City College of the City University of New York, New York, New York 10031

Abraham Nitzan[a)]

Bell Telephone Laboratories, Murray Hill, New Jersey 07974
(Received 27 March 1980; accepted 21 May 1980)

A theory for surface enhanced Raman scattering (SERS) is developed. Effects due to realistic surface geometry and dielectric properties are included. Three sources of enhanced Raman scattering are noted: the image dipole enhancement effect, the increase of local field ("lightning rod" effect), and the resonant excitation of surface plasmons. The surface is modeled as a hemispheroid protruding from a conducting plane, although other models are considered. The spherical limit is discussed in some detail and molecular orientation effects are considered. Cross sections for Mie, Rayleigh, and Raman scattering are derived.

I. INTRODUCTION

The observation[1-3] of surface enhanced Raman scattering (SERS) of molecules adsorbed on some metal electrodes has led to a mounting experimental and theoretical effort aimed at elucidating the nature of the phenomenon.[4] It has recently been observed[5] that the phenomenon persists on rough metallic surfaces in high vacuum. A broad range of theoretical models has been advanced to explain the effect.[4]

Recent experimental results[6] indicate that the SERS phenomenon persists beyond the first layer of adsorbed molecules: the surface effect appears to decrease slowly with the distance from the surface (over a length scale of 10–100 Å). It was also noticed that the presence of large scale surface roughness appears to be necessary to observe the enhancement.

It should be kept in mind that more than one mechanism may be responsible for the enhancement phenomenon and that the observed enhancement factors result from a combination of several contributions. One may not exclude the possibility that chemical interactions, e.g., formation of charge transfer states of the metal-adsorbed molecule complex[7] are effective at close range. However the apparent long range nature of the phenomenon suggests that electromagnetic interactions are of primary importance. This stands in accord with the suggestion made by Moscovits[8] that the excitation of transverse collective electron resonances associated with microscopic bumps on the metal surface is responsible for the enhancement. Burstein *et al.*[9] have developed this idea and pointed out that the increase in the local electric field at the surface near such a resonance gives rise to an apparent enhanced Raman scattering by the molecule which is subjected to this increased field.

Another source for enhancement which is not related to excitation of surface resonances occurs when the molecule is adsorbed near high curvature edges of surface irregularities. The polarization of the metal in the external electric field produces a strong local field in the vicinity of such edges which in turn appears as an enhanced Raman scattering by the molecule experiencing this field. This "lightning rod mechanism" was recently proposed[10] for perfectly conducting ellipsoidal metal particles. Very large enhancement ratios may be obtained for a molecule adsorbed along the long axis of such an ellipsoid.

In practice both the resonances and the lightning rod effect are operative in principle. In addition to those the image enhancement mechanism[11,12] may be effective at close range and the polarization of the metal by the molecular dipole (which also contributes to the Raman scattering component) should also be taken into account. This is the subject of this paper: we explore the effects on the Raman scattering by a molecule associated with the electromagnetic interaction of this molecule with small metal particles or small surface imperfections located nearby. Classical electrodynamics is used throughout, with the molecule represented by a polarizable point dipole and the metal—by a continuous medium of specified shape and a dielectric constant $\epsilon(\omega)$.

The effect of the electromagnetic interaction between the molecule of interest and a polarizable body located close to it on the Raman scattering by the molecule may be illustrated by the following simple model: The molecule is represented by a point dipole μ_1 induced by the external electric field $\mathbf{E}$ with the corresponding molecular polarizability tensor α_1

$$\mu_1 = \alpha_1 \cdot \mathbf{E} \,. \tag{1.1}$$

A second body (e.g., an atom) is similarly represented by μ_2 and α_2. The electric field $\mathbf{E}$ is composed of a part $\mathbf{E}_0$ associated with the incident radiation and a contribution from the induced dipoles. This leads to the following set of coupled equations:

$$\mu_1 = \alpha_1 \cdot (\mathbf{E}_0 + \mathbf{M} \cdot \mu_2) \,, \tag{1.2a}$$

$$\mu_2 = \alpha_2 \cdot (\mathbf{E}_0 + \mathbf{M} \cdot \mu_1) \,, \tag{1.2b}$$

where

$$\mathbf{M} = (3\hat{n}\hat{n} - \mathbf{1})/d^3 \,, \tag{1.3}$$

with $\mathbf{d}$ being the distance vector between the two dipoles,

[a)] On leave from the Department of Chemistry, Tel Aviv University, Tel Aviv, Israel.

 0021-9606/80/193023-15$01.00 © American Institute of Physics

Downloaded 15 Feb 2004 to 132.66.16.12. Redistribution subject to AIP license or copyright, see http://jcp.aip.org/jcp/copyright.jsp

$\hat{n}=\mathbf{d}/d$, and $\mathbf{I}$ is the unit tensor. The quantities μ_1, μ_2, and $\mathbf{E}_0$ are the (complex) amplitudes of the corresponding oscillating dipoles and field [coefficients of $\exp(-i\omega t)$] and the polarizabilities α_1 and α_2 are in principle ω dependent. The validity of Eq. (1.2) is limited to the case where $d \ll 2\pi c/\omega$, where c is the speed of light. For larger d values retardation effects are important.

Solving Eqs. (1.2) for μ_1, we obtain

$$\mu_1 = [\mathbf{I} - \alpha_1 \cdot \mathbf{M}(d) \cdot \alpha_2 \cdot \mathbf{M}(d)]^{-1} \cdot \alpha_1 \cdot [\mathbf{I} + \mathbf{M}(d) \cdot \alpha_2] \cdot \mathbf{E}_0 . \tag{1.4}$$

The effective polarizability of the molecule is

$$\alpha_1^{\mathrm{eff}} = [\mathbf{I} - \alpha_1 \cdot \mathbf{M} \cdot \alpha_2 \cdot \mathbf{M}]^{-1} \cdot \alpha_1 \cdot [\mathbf{I} + \mathbf{M} \cdot \alpha_2] . \tag{1.5}$$

Similarly,

$$\alpha_2^{\mathrm{eff}} = [\mathbf{I} - \alpha_2 \cdot \mathbf{M} \cdot \alpha_1 \cdot \mathbf{M}]^{-1} \cdot \alpha_2 \cdot [\mathbf{I} + \mathbf{M} \cdot \alpha_1] . \tag{1.6}$$

In this classical picture the Raman polarizability is associated with the nuclear coordinate dependence of α_1. Obviously both α_1^{eff} and α_2^{eff} carry such contributions. The total Raman polarizability is

$$\alpha_{\mathrm{RAM}}^{\mathrm{tot}} = \Delta Q \frac{\partial}{\partial Q} [\alpha_1^{\mathrm{eff}} + \alpha_2^{\mathrm{eff}}] , \tag{1.7}$$

where Q is the amplitude of the relevant nuclear coordinate. Equation (1.7) is based on the fact that both dipoles occupy essentially the same spatial location as far as the scattering process is concerned. Equations (1.5)–(1.7) yield

$$\alpha_{\mathrm{RAM}}^{\mathrm{tot}} = \Delta Q (\mathbf{I} - \alpha_1 \cdot \mathbf{M} \cdot \alpha_2 \cdot \mathbf{M})^{-1} \left(\frac{\partial \alpha_1}{\partial Q} \cdot [\mathbf{M} \cdot \alpha_2 \cdot \mathbf{M} (\mathbf{I} - \alpha_1 \cdot \mathbf{M} \cdot \alpha_2 \cdot \mathbf{M})^{-1} + \mathbf{I}][\mathbf{I} + \mathbf{M} \cdot \alpha_2] + \alpha_2 \cdot \mathbf{M} \cdot \frac{\partial \alpha_1}{\partial Q} \cdot [\mathbf{M} \cdot (\mathbf{I} - \alpha_1 \cdot \mathbf{M} \cdot \alpha_2 \cdot \mathbf{M})^{-1} \cdot \alpha_2 \cdot (\mathbf{I} + \mathbf{M} \cdot \alpha_1) + \mathbf{I}] \right) . \tag{1.8}$$

The differential Raman scattering cross section is

$$\frac{d\sigma}{d\Omega} = k^4 |\hat{e} \cdot \alpha_{\mathrm{RAM}}^{\mathrm{tot}} \cdot \hat{e}_0|^2 , \tag{1.9}$$

where Ω is the angle denoting a particular direction in space, $k=\omega/c$, and where $\hat{e}_0$ and $\hat{e}$ are the polarization vectors of the incident and scattered radiation. Inspection of expressions (1.5), (1.6), and (1.7) reveals three sources for the effect of a (closely lying) polarizable body on the Raman scattering of the molecule:

(i) The polarization of the body in the external field leads to an induced local field ($\mathbf{M} \cdot \alpha_2 \cdot \mathbf{E}_0$) which adds to the oscillating field seen by the molecule ("local field effect").

(ii) The polarization of the body by the induced oscillating molecular dipole induces an additional oscillating field felt by the molecule ("image effect").

(iii) The polarization of the body by the induced molecular dipole has a Raman component and contributes to the Raman scattering.

The "image effect" is associated with the inverse matrices appearing in Eqs. (1.5), (1.6), and (1.8). These inverses are essentially of the order $(1-\alpha_1\alpha_2 d^{-6})^{-1}$ and can give rise to enhanced scattering when the distance R is small enough so that $\alpha_1\alpha_2 d^{-6}$ is close to unity. Similar observations lead to the image mechanism for SERS proposed in several works.[11,12] We should keep in mind, however, that the polarizabilities α_1 and α_2 are normally of the orders of the corresponding molecular volumes and that the point dipole model is valid only provided that these volumes are much smaller than d^3. Also, distances for which $\alpha_1\alpha_2 d^{-6} \sim 1$ are so small that the classical picture itself becomes questionable. Finally the recent experimental results of the Bell group[6] suggest that at least part of the SERS effect is relatively long range in nature and persists at distances for which the image contribution is negligible.

Disregarding the image effect results in a much simpler expression for the total Raman polarizability

$$\alpha_{\mathrm{RAM}}^{\mathrm{tot}} = \Delta Q \left[\frac{\partial \alpha_1}{\partial Q} + \frac{\partial \alpha_1}{\partial Q} \cdot \mathbf{M} \cdot \alpha_2 + \alpha_2 \cdot \mathbf{M} \cdot \frac{\partial \alpha_1}{\partial Q} \right] . \tag{1.10}$$

Of the three terms appearing on the right-hand side of Eq. (1.10), the first corresponds to the Raman scattering by the free molecule, the second corresponds to the additional Raman scattering by the molecule due to the local field induced by the body, and the third is related to the Raman component of the polarization induced on the body by the molecular field. Equation (1.10) implies that the Raman scattering of this system will be substantially enhanced relative to that of the free molecule if $||\mathbf{M} \cdot \alpha_2|| \gg 1$. This is essentially equivalent to

$$||\alpha_2/d^3|| \gg 1 . \tag{1.11}$$

This inequality may hold if one or both of the following conditions are satisfied:

(i) The incident frequency is close to a resonance of the body which may couple to the incident field. $\alpha_2(\omega)$ is large near such a resonance.

(ii) The size and the geometrical shape of the body are such that α_2 is large even for a static field ($\omega = 0$).

Manifestations of both possibilities will be seen in the more realistic examples considered in the following sections. In particular when the body is a small metal particle or a small metallic surface imperfection, the relevant resonances are identified as the surface plasmon resonances of this particle while the size and shape of the particle enter through the "lightning rod effect": the establishment of a strong electric field near surfaces of large curvatures.

In Sec. II we consider a model for a molecule adsorbed on a surface imperfection. The latter is taken to be a prolate hemispheroid with the semimajor axis perpen-

Downloaded 15 Feb 2004 to 132.66.16.12. Redistribution subject to AIP license or copyright, see http://jcp.aip.org/jcp/copyright.jsp

dicular to the surface and the molecular dipole lying above the surface along this axis and parallel to it. The model is simplified by assuming that the surface is a perfect conductor [while the hemispheroid is characterized by a dielectric function $\epsilon(\omega)$]. A comparison with the corresponding solution for an isolated complete spheroid reveals that the nature of the planar surface plays only a secondary role in the Raman enhancement effect.

Section II discusses only electric dipole scattering. In Sec. III the possible role of magnetic dipole scattering is discussed within the same model. In Sec. IV we analyze the Raman enhancement ratio associated with this model and its dependence on physical parameters (metal particle shape, molecule–surface distance, and incident radiation frequency). Finally, in Sec. V we remove, for the particular case of a molecule adsorbed on a metal sphere, the restrictions imposed on the molecule orientation relative to the sphere and on the orientation of the molecule–sphere complex in the electromagnetic field, and evaluate for this example the complete Raman polarizability tensor. From this we obtain the directionality properties of the enhancement effect and the polarization of the scattering light.

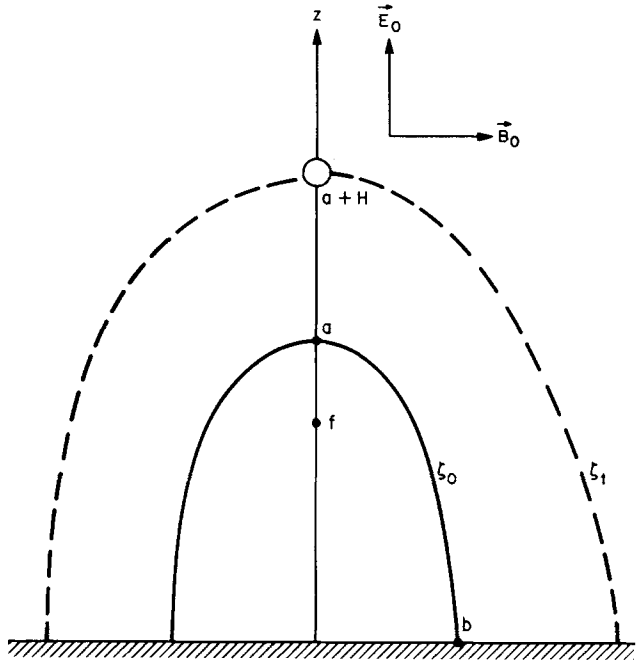

FIG. 1. Geometry of surface protrusion. The semimajor axis is a and the semiminor axis is b. The spheroid surface is $\xi = \xi_0$ and that surface passing through the molecule is $\xi = \xi_1$.

II. POLARIZABILITY OF A MOLECULE ADSORBED ON A SPHEROIDAL SURFACE IMPERFECTION

Let us compute the light scattering produced when a laser field is incident on a molecule adsorbed on a rough surface. The surface will be taken to be a prolate hemispheroid protruding from a flat plane. The molecule is taken to be along the symmetry axis some distance above the spheroid. The spheroid is assumed to have the complex dielectric constant $\epsilon(\omega)$, while the plane is taken to be a perfect conductor. This latter assumption allows for a great mathematical simplification of the electrostatic problem while, as we shall see below, it has only a secondary effect on the Raman scattering process. The incident electric field is taken to be along the symmetry axis, and the molecular dipole is taken to be along this axis and parallel to it. The geometric arrangement is depicted in Fig. 1.

We shall make the assumption that the wavelength of the light is much larger than the semimajor axis of the spheroid a and the molecule–surface distance H. Ordinarily one must solve the Helmholtz equation for the field variables, e.g.,

$$(\nabla^2 + k^2)\mathbf{E} = 0 , \tag{2.1}$$

but if kH, $ka \ll 1$, this reduces to the Laplace equation

$$\nabla^2 \mathbf{E} = 0 . \tag{2.2}$$

The problem is thus reduced to the study of a static field configuration.

Let us first consider the electrostatic problem. In the region outside the spheroid we have an applied external field, a polarized molecule producing an electric field, and a field due to the spheroid and the plane. The potential may be written in the following form:

$$\Phi_{\mathrm{I}} = -E_0 f \xi\eta + \frac{\mu}{f^2}\frac{\partial}{\partial \xi_1}\left\{[(\xi^2-1)(1-\eta^2) + (\xi\eta - \xi_1)^2]^{-1/2} - [(\xi^2-1)(1-\eta^2) + (\xi\eta + \xi_1)^2]^{-1/2}\right\} + \sum_n{}' c_n P_n(\eta) Q_n(\xi) . \tag{2.3}$$

P_n and Q_n denote Legendre functions of the first and second kind, respectively. Inside the spheroid we simply write down a general solution to the Laplace equation

$$\Phi_{\mathrm{II}} = \sum_n{}' b_n P_n(\eta) P_n(\xi) . \tag{2.4}$$

In Eqs. (2.3) and (2.4) we have introduced the spheroidal coordinates

$$\begin{aligned} x &= f[(\xi^2-1)(1-\eta^2)]^{1/2}\cos\phi , \\ y &= f[(\xi^2-1)(1-\eta^2)]^{1/2}\sin\phi , \\ z &= f\xi\eta , \end{aligned} \tag{2.5}$$

where the ϕ is an azimuthal coordinate and ξ and η are the orthogonal spheroidal coordinates. The focal distance f is related to the semimajor axis a and semiminor axis b by

$$f = (a^2 - b^2)^{1/2} . \tag{2.6}$$

The surface of the spheroidal protrusion is $\xi = \xi_0$, where

$$\xi_0 = a/f . \tag{2.7}$$

The molecule is located a distance H above the spheroid and lies on the surface

$$\xi_1 = (a + H)/f . \tag{2.8}$$

In Eq. (2.3) we have included in the second term a contribution from the polarized molecule, whose dipole μ

Downloaded 15 Feb 2004 to 132.66.16.12. Redistribution subject to AIP license or copyright, see http://jcp.aip.org/jcp/copyright.jsp

is assumed to be parallel to $\mathbf{E}_0$, and a contribution from its image a distance $a+H$ below the plane. The last term in Eq. (2.3) represents the general solution to Laplace's equation which is well behaved at $\eta=1$ and $\xi=\infty$. It represents the potential associated with the polarized hemispheroid and its surface image on the conducting plane. The potential Φ_I is chosen so that it vanishes on the plane of the flat surface ($\eta=0$). Thus only odd n terms appear in the summation. This is true also for the potential inside the spheroid, given by Eq. (2.4). Equation (2.4) represents the most general solution to the Laplace equation which is well behaved at $\xi=1$ and $\eta=1$.

The coefficients a_n and b_n must be determined by matching the two solutions at the boundary $\xi=\xi_0$ for all η in the range $0\leq\eta\leq 1$. If we impose the condition that Φ is continuous across this surface we obtain

$$-E_0 f\xi\eta+\frac{\mu}{f^2}\frac{\partial}{\partial\xi_1}\{[(\xi_0^2-1)(1-\eta^2)+(\xi_0\eta-\xi_1)^2]^{-1/2} - [(\xi_0^2-1)(1-\eta^2)+(\xi_0\eta+\xi_1)^2]^{-1/2}\} = \sum_n{}' [b_n P_n(\xi_0)-c_n Q_n(\xi_0)]P_n(\eta) . \quad (2.9)$$

If we match the normal components of the displacement vectors along this surface we obtain

$$-E_0 f\eta+\frac{\mu}{f^2}\frac{\partial^2}{\partial\xi_0\partial\xi_1}\{[(\xi_0^2-1)(1-\eta^2)+(\xi_0\eta-\xi_1)^2]^{-1/2} - [(\xi_0^2-1)(1-\eta^2)+(\xi_0\eta+\xi_1)^2]^{-1/2}\} = \sum_n{}' [\epsilon(\omega)b_n P_n'(\xi_0)-c_n Q_n'(\xi_0)]P_n(\eta) . \quad (2.10)$$

These expressions may be inverted to obtain the coefficients b_n and c_n by employing the integral

$$\int_0^1 P_n(\eta)P_m(\eta)\,d\eta=\frac{\delta_{mn}}{2n+1} , \quad (2.11)$$

which is valid for m and n both odd, and the integral

$$\int_0^1 P_n(\eta)\{1/[(\xi_0^2-1)(1-\eta^2)+(\xi_0\eta-\xi_1)^2]^{1/2} - 1/[(\xi_0^2-1)(1-\eta^2)+(\xi_0\eta+\xi_1)^2]^{1/2}\}d\eta = 2P_n(\xi_0)Q_n(\xi_1) , \quad (2.12)$$

when n is odd and $\xi_1>\xi_0>1$. Thus we obtain the equation

$$b_n P_n(\xi_0)-c_n Q_n(\xi_0)=-E_0 f\xi_0\delta_{n,1} + (4n+2)(\mu/f^2)P_n(\xi_0)Q_n'(\xi_1) , \quad (2.13a)$$

and

$$\epsilon(\omega)b_n P_n'(\xi_0)-c_n Q_n'(\xi_0) = -E_0 f\delta_{n,1}+(4n+2)(\mu/f^2)P_n'(\xi_0)Q_n'(\xi_1) . \quad (2.13b)$$

Solving these for C_n gives

$$c_n=\frac{(\epsilon-1)E_0 f\xi_0\delta_{n,1}}{\epsilon Q_1(\xi_0)-\xi_0 Q_1'(\xi_0)}+\frac{(4n+2)\mu}{f^2} \times\frac{(1-\epsilon)P_n'(\xi_0)Q_n'(\xi_1)P_n(\xi_0)}{\epsilon Q_n(\xi_0)P_n'(\xi_0)-Q_n'(\xi_0)P_n(\xi_0)} . \quad (2.14)$$

In the long wavelength limit the dominant electrical emission is due to the dipole moment. By examining Eq. (2.3) for large ξ, we may isolate the electrical dipole moment D:

$$\Phi_I \xrightarrow[\xi\to\infty]{} \frac{D\eta}{(f\xi)^2}-E_0 f\xi\eta , \quad (2.15)$$

where

$$D=2\mu+\tfrac{1}{3}c_1 f^2 . \quad (2.16)$$

The 2μ term is just the sum of the molecular dipole and its image in the plane. The second term is the dipole induced on the spheroid (and its image in the plane). Thus we find

$$D=\frac{f^3E_0}{3}\frac{\xi_0(\epsilon-1)}{\epsilon Q_1(\xi_0)-\xi_0Q_1'(\xi_0)} + 2\mu\left(1+\frac{(1-\epsilon)\xi_0Q_1'(\xi_1)}{\epsilon Q_1(\xi_0)-\xi_0Q_1'(\xi_0)}\right) . \quad (2.17)$$

In general a molecule has a polarizability tensor which is anisotropic. Let us assume that the molecule is oriented so that one of the principal axes is oriented along the z axis. The polarizability along this direction is denoted by α. The dipole is then determined by the net electrical field produced at the molecule's position by the spheroid, the plane, and the external field. Thus

$$\mu=\alpha\left(-\frac{1}{f}\sum_n{}' c_n Q_n'(\xi_1)+\frac{\mu}{4(f\xi_1)^3}+E_0\right) . \quad (2.18)$$

Combining Eqs. (2.17) and (2.18) leads to the expression

$$D=\frac{f^3E_0}{3}\frac{\xi_0[\epsilon(\omega)-1]}{\epsilon(\omega)Q_1(\xi_0)-\xi_0Q_1'(\xi_0)} + \frac{2\alpha E_0}{1-\Gamma}\left(1+\frac{[1-\epsilon(\omega)]\xi_0Q_1'(\xi_1)}{\epsilon(\omega)Q_1(\xi_0)-\xi_0Q_1'(\xi_0)}\right)^2 , \quad (2.19)$$

where

$$\Gamma=\frac{\alpha}{4(f\xi_1)^3}+\frac{2\alpha[\epsilon(\omega)-1]}{f^3} \times\sum_n{}' \frac{(2n+1)P_n(\xi_0)P_n'(\xi_0)[Q_n'(\xi_1)]^2}{\epsilon(\omega)P_n'(\xi_0)Q_n(\xi_0)-P_n(\xi_0)Q_n'(\xi_0)} . \quad (2.20)$$

In Eq. (2.19), the first term, which is independent of α and ξ, is the contribution to the dipole moment due to an isolated hemispheroid on a conducting plane. The second term is the effect of the molecule.

The denominator $1-\Gamma$ appearing in Eq. (2.19) may be termed the image enhancement factor. Γ consists of two terms, one due to the image of the molecular dipole in the plane and the second due to its image in the hemispheroid. To see this suppose we take the limit $\epsilon(\omega)\to -1$, i.e., eliminate the hemispheroid entirely. Then $\Gamma\to 2\alpha/[2(a+H)]^3$, where use has been made of Eq. (2.8). This is the familiar expression for the image enhancement term for a molecule near a plane. Further insight is obtained by examining the second term in Eq. (2.20) in the case where the hemispheroid is also a perfect conductor. Thus let $|\epsilon(\omega)|\to\infty$ and then Γ becomes

$$\Gamma_\infty=\frac{\alpha}{4(f\xi_1)^3}+\frac{2\alpha}{f^3}\sum_n{}' (2n+1)\frac{P_n(\xi_0)[Q_n'(\xi_1)]^2}{Q_n(\xi_0)} . \quad (2.21)$$

Downloaded 15 Feb 2004 to 132.66.16.12. Redistribution subject to AIP license or copyright, see http://jcp.aip.org/jcp/copyright.jsp

Consider the case where the molecule is close to the surface, i.e., $\xi_1 \approx \xi_0$. If our intuition is correct, then as we make the ellipsoid less eccentric (increase ξ_0 towards infinity) the ellipsoid will look locally like a plane and the second term should reduce to $2\alpha/(2H)^3$. This is indeed obtained by the use of the asymptotic formulas ($\xi_1 > \xi_0 \gg 1$)

$$Q_n(\xi_0) \underset{\xi_0 \to \infty}{\longrightarrow} \frac{\pi^{1/2} n!}{2^{n+1}\Gamma(n+\frac{3}{2})\xi_0^{n+1}} , \tag{2.22}$$

where $\Gamma(x)$ is the gamma function, and

$$P_n(\xi_0) \underset{\xi_0 \to \infty}{\longrightarrow} \frac{2^n \Gamma(n+\frac{1}{2})\xi_0^n}{\pi^{1/2} n!} , \tag{2.23}$$

when

$$\frac{2\alpha}{f^3}\sum{}' (2n+1)\frac{P_n(\xi_0)}{Q_n(\xi_0)}[Q_n'(\xi_1)]^2 \rightarrow \frac{2\alpha\xi_0}{f^3\xi_1^4}\sum{}' (n+1)^2\left(\frac{\xi_0}{\xi_1}\right)^{2n} \rightarrow \frac{2\alpha}{(2H)^3} , \tag{2.24}$$

as expected. For a finite geometry, of course, the expressions in Eqs. (2.20) and (2.21) will differ from the predictions of the plane image enhancement theory. For $a, b \gg H$ the plane image expression provides a convenient approximation.

For the perfectly conducting hemiellipsoid on a conducting plane Eq. (2.19) reduces to

$$D_\infty = \frac{f^3 E_0 \xi_0}{3Q_1(\xi_0)} + \frac{2\alpha E_0}{1-\Gamma_\infty}\left(1 - \frac{\xi_0 Q_1'(\xi_1)}{Q_1(\xi_0)}\right)^2 , \tag{2.25}$$

where Γ_∞ is defined in Eq. (2.21). It is worthwhile comparing these results to the case where the spheroids are totally isolated, i.e., no conducting plate and a full rather than a hemispheroid. Equation (2.3) is modified so that there is no image dipole term associated with the plane and the sum is extended over all values of n. The potentials are now matched over the entire range $-1 \le \eta \le 1$. We then find

$$\tilde{D} = \frac{f^3 E_0}{3}\frac{\xi_0[\epsilon(\omega)-1]}{\epsilon(\omega)Q_1(\xi_0) - \xi_0 Q_1'(\xi_0)} + \frac{\alpha E_0}{1-\tilde{\Gamma}}\left(1 + \frac{[1-\epsilon(\omega)]\xi_0 Q_1'(\xi_1)}{\epsilon(\omega)Q_1(\xi_0) - \xi_0 Q_1'(\xi_0)}\right)^2 , \tag{2.26}$$

where

$$\tilde{\Gamma} = \frac{\alpha}{f^3}[\epsilon(\omega)-1]\sum_n \frac{(2n+1)P_n(\xi_0)P_n'(\xi_0)[Q_n'(\xi_1)]^2}{\epsilon(\omega)P_n'(\xi_0)Q_n(\xi_0) - P_n(\xi_0)Q_n'(\xi_0)} . \tag{2.27}$$

In the perfect conductor limit [$|\epsilon(\omega)| \to \infty$], these simplify to results obtained previously[10]

$$\tilde{D}_\infty = \frac{f^3 E_0 \xi_0}{3Q_1(\xi_0)} + \frac{\alpha E_0}{1-\tilde{\Gamma}_\infty}\left(1 - \frac{\xi_0 Q_1'(\xi_0)}{Q_1(\xi_0)}\right)^2 , \tag{2.28}$$

where

$$\tilde{\Gamma}_\infty = \frac{\alpha}{f^3}\sum_{n=0}^{\infty}(2n+1)\frac{P_n(\xi_0)}{Q_n(\xi_0)}[Q_n'(\xi_1)]^2 , \tag{2.29}$$

Comparison of Eqs. (2.26) and (2.27) with (2.19) and (2.20) show them to be of the same basic structure with some slight numerical differences (see Fig. 8).

Equations (2.19) and (2.26) contain denominator terms of the form

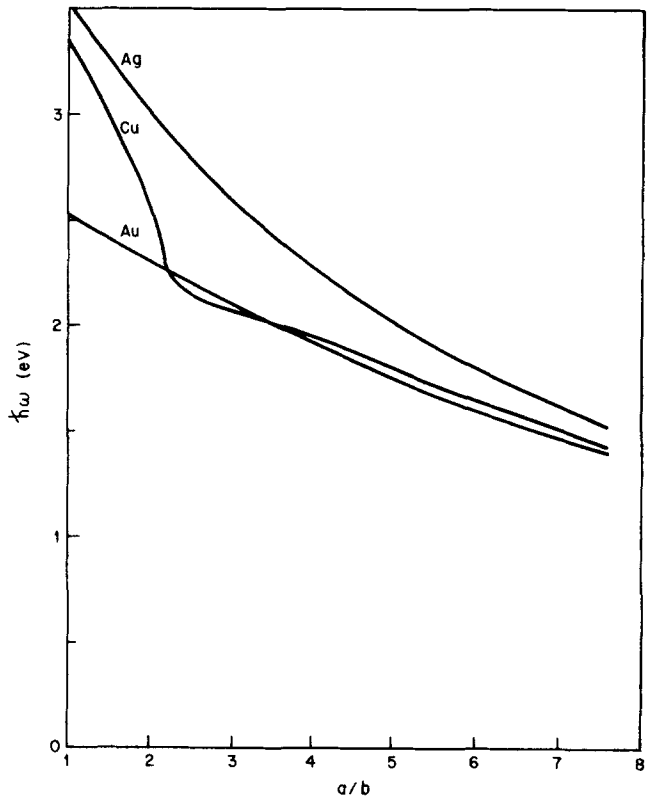

FIG. 2. Energy of surface plasmons for Ag, Cu, and Au as a function of the aspect ratio a/b of the spheroid.

$$\Delta(\xi_0, \omega) = \epsilon(\omega)Q_1(\xi_0) - \xi_0 Q_1'(\xi_0) . \tag{2.30}$$

The zero of this expression is the condition for a surface plasmon of the spheroid. In the limit as $\xi_0 \to \infty$, in which the spheroid tends towards a sphere, Δ simplifies to

$$\Delta(\xi_0, \omega) \underset{\xi_0 \to \infty}{\longrightarrow} \frac{\epsilon(\omega)+2}{3\xi_0^2} . \tag{2.31}$$

The condition for a surface plasmon of a sphere is

$$\epsilon(\omega) + (l+1)/l = 0 , \tag{2.32}$$

so for $l=1$ (dipole case), this reduces to $\epsilon(\omega)+2=0$.

In the highly prolate limit ($\xi_0 \to 1$), the zero of Eq. (2.30) occurs when

$$\epsilon(\omega) = \{(\xi_0 - 1)\ln[2/(\xi_0 - 1)]\}^{-1} , \tag{2.33}$$

which means that $\epsilon(\omega)$ will be large and negative.

In Fig. 2 the surface plasmon frequency is plotted as a function of the aspect ratio a/b for Ag, Cu, and Au. The optical data of Johnson and Christy[13] was employed to find the frequency corresponding to a given value of ϵ. For $a/b = 1$ we obtain the spherical surface plasmon energy of 3.50 eV. This is below the value for a flat surface where $\hbar\omega_s = 3.68$ eV (i.e., $\epsilon + 1 = 0$). Both values are below the bulk plasma frequency $\hbar\omega_B = 3.81$ eV (where $\epsilon = 0$). As the spheroid becomes more eccentric the surface plasmon frequency gets lower. Thus a laser at a given frequency will select spheroids of a given aspect ratio to be in resonance with. From the form of Eq. (2.19) we may expect a strong enhancement in D in the neighborhood of such a resonance. A necessary condition is obviously that $\mathrm{Im}\epsilon(\omega)$ be small at the resonance

Downloaded 15 Feb 2004 to 132.66.16.12. Redistribution subject to AIP license or copyright, see http://jcp.aip.org/jcp/copyright.jsp

frequency when $\mathrm{Re}\epsilon(\omega)$ satisfies Eq. (2.30). The fact that Ag satisfies this condition best explains its high efficiency in the SERS effect.

We note in passing that when a sphere is distorted to become a spheroid its dipolar surface plasmon splits as may be seen from the polarizability tensor of the ellipsoid

$$\alpha_{\text{ellipsoid}}=\begin{pmatrix}\alpha^{(1)} & 0 & 0\\ 0 & \alpha^{(2)} & 0\\ 0 & 0 & \alpha^{(3)}\end{pmatrix}, \tag{2.34}$$

where

$$\alpha^{(1)}=\alpha^{(2)}=-\frac{2(\epsilon-1)f^3\xi_0}{3[Q_1^1(\xi_0)P_1^{1\prime}(\xi_0)-Q_1^{1\prime}(\xi_0)P_1^1(\xi_0)]} \tag{2.35}$$

and

$$\alpha^{(3)}=\frac{(\epsilon-1)f^3\xi_0}{3[\epsilon Q_1(\xi_0)-\xi_0 Q_1'(\xi_0)]}\ . \tag{2.36}$$

Equation (2.36) is obtained from the α independent term of Eq. (2.26), while Eq. (2.35) in which Q_1^1 and P_1^1 are associated Legendre functions may be obtained from a similar calculation as above with the external field perpendicular to the spheroid major axis. We now expand Eqs. (2.35) and (2.36) about the sphere limit defined by

$$\begin{aligned}&f\to 0\ ,\quad \xi_0\to\infty\ ,\\ &f^3\xi_0(\xi_0^2-1)=ab^2=\text{const}\equiv\bar{a}^3\ ,\end{aligned} \tag{2.37}$$

and obtain

$$\alpha^{(1)}=\alpha^{(2)}=\frac{(\epsilon-1)\bar{a}^3}{\epsilon+2+\frac{2}{10}(\epsilon-1)[(a/\bar{a})^2-1]} \tag{2.38}$$

and

$$\alpha^{(3)}=\frac{(\epsilon-1)\bar{a}^3}{\epsilon+2-\frac{3}{5}(\epsilon-1)[(a/\bar{a})^2-1]}\ . \tag{2.39}$$

The sphere dipolar surface plasmon resonance is seen to split into two: For metals like Ag, Cu, and Au, the resonance in $\alpha^{(3)}$ occurs at lower energies and that in $\alpha^{(1)}=\alpha^{(2)}$—at higher energies than the corresponding sphere resonance. When the molecule is adsorbed along the spheroid major axis with the induced dipole parallel to this axis (which is the model considered here), only $\alpha^{(3)}$ plays a role in the α (molecular polarizability) dependent part of the total induced dipole D.

Equations (2.19), (2.20) (for the hemispheroid on a conducting surface) and (2.26), (2.27) (for the full spheroid) constitute the final expressions for the dipole induced in the system by an external electric field. The coefficients of $\mathbf{E}_0$ in the expression for D [Eq. (2.19)] and $\bar{D}$ [Eq. (2.20)] are the corresponding polarizabilities. Their α-dependent parts give rise to the Raman polarizability via the nuclear coordinate dependence of α. Before proceeding in evaluating the Raman scattering intensity we briefly discuss the possible role of magnetic scattering.

III. MAGNETIC SCATTERING

In this section we consider the effect of magnetic dipole scattering from the hemiellipsoid on the conducting plane. We shall not treat the problem in its fullest generality but rather consider two limiting, but useful, cases.

In the first case consider Maxwell's equations in the ellipsoid

$$\nabla\times\mathbf{E}=(i\omega/c)\mathbf{B}\ , \tag{3.1a}$$

$$\nabla\times\mathbf{H}=(-i\omega\epsilon/c)\mathbf{E}\ , \tag{3.1b}$$

$$\nabla\cdot\mathbf{B}=0\ , \tag{3.1c}$$

$$\nabla\cdot\epsilon\mathbf{E}=0\ . \tag{3.1d}$$

We will assume the magnetic susceptibility of the metal is unity so $\mathbf{B}=\mathbf{H}$. In the limit $\omega a/c\ll 1$, in plane of the first equation we have

$$\nabla\times\mathbf{E}=0\ , \tag{3.1a'}$$

and the electric field is obtained by solving the appropriate electrostatic problem, as in the previous section. The Ampere law, however, may not be trucated unless one imposes the condition

$$|a\omega\epsilon/c|\ll 1\ . \tag{3.2}$$

If this is true then

$$\nabla\times\mathbf{B}\to 0\ , \tag{3.1b'}$$

and we find that the magnetic field satisfies Laplace's equation everywhere. Then $\mathbf{B}=\mathbf{B}_0$ is the solution, where $\mathbf{B}_0$ is the incident laser magnetic field. In this limit no magnetic scattering occurs.

In the second limiting case we may imagine that the magnitude of ϵ is sufficiently large that

$$|b\omega\epsilon/c|\gg 1\ . \tag{3.3}$$

Then the metal is behaving like a perfect conductor so, from Eq. (3.1b), $\mathbf{E}=0$. Then, from Eqs. (3.1a) and (3.1c), $B_\xi=0$ on the surface of the conductor. Outside the conductor we have

$$\mathbf{B}=-\nabla\psi\ , \tag{3.4}$$

where ψ is the magnetostatic poential. The magnetic potential may be written

$$\begin{aligned}\psi=&-B_0 f[(\xi^2-1)(1-\eta^2)]^{1/2}\cos\phi\\ &+\gamma Q_1^1(\xi)(1-\eta^2)^{1/2}\cos\phi\ ,\end{aligned} \tag{3.5}$$

where $Q_1^1(\xi)$ is an associated Legendre function of the second kind. Imposition of the boundary condition that $B_\xi=0$ at $\xi=\xi_0$ yields

$$\gamma=B_0 f\xi_0/[Q_1(\xi_0)+(\xi_0^2-1)^{-1}]\ . \tag{3.6}$$

The magnetic dipole is

$$m=-\tfrac{2}{3}f^2\gamma\ , \tag{3.7}$$

as may be seen by expanding Eq. (3.5) in powers of $1/\xi$. In the sphere limit ($\xi_0\gg 1$) this reduces to the familiar expression

$$m\xrightarrow[\xi_0\to\infty]{}\tfrac{1}{2}a^3B_0\ . \tag{3.8}$$

In the needle limit

$$m\xrightarrow[\xi_0\to 1]{}-\tfrac{1}{3}f^3B_0(\xi_0-1)\ , \tag{3.9}$$

which shows that magnetic scattering is not important

Downloaded 15 Feb 2004 to 132.66.16.12. Redistribution subject to AIP license or copyright, see http://jcp.aip.org/jcp/copyright.jsp

for highly prolate objects of our given geometry.

One may generalize the magnetic dipole expression and write

$$m = -\frac{2B_0}{3}\frac{f^3\xi_0 F}{Q_1(\xi_0)+(\xi_0^2-1)^{-1}} , \tag{3.10}$$

where F is a factor which is 1 if Eq. (3.3) is obeyed and is 0 if Eq. (3.2) is obeyed. For intermediate values it interpolates between these extremes in a yet undetermined manner.

IV. THE SCATTERING CROSS SECTION

Let us now compute the dipole radiation produced when an incident laser field directed along the symmetry axis strikes the roughness configuration as in Fig. 1. We note that in actual experiments the incident electric field is not usually oriented along the symmetry axis of Fig. 1. (It may be so oriented if Fig. 1 represents a local configuration not parallel to the macroscopic surface.) Surface currents induced by the parallel component of the field may modify the results presented here which include only the effect of the protrusions plus their images in the substrate surface.

The total radiated power is given by Larmor's formula in the dipole approximation

$$P = (\omega^4/3c^3)(D^2+m^2) , \tag{4.1}$$

where D is given by Eq. (2.19) and m is given by Eq. (3.10). Dividing this expression by the incident intensity $CE_0^2/8\pi$ yields an expression for the elastic light scattering cross section

$$\sigma = \sigma_M + \sigma_R + \sigma_{RM} , \tag{4.2}$$

where σ_M is the Mie scattering cross section

$$\sigma_M = \frac{8\pi}{27}\left(\frac{\omega}{c}\right)^4 f^6\xi_0^2\left(\frac{|\epsilon-1|^2}{|\epsilon Q_1(\xi_0)-\xi_0 Q_1'(\xi_0)|^2} + \frac{4F^2}{[Q_1(\xi_0)+(\xi_0^2-1)^{-1}]^2}\right) , \tag{4.3}$$

which is independent of the molecule; σ_R is the Rayleigh scattering cross section resulting from the presence of the molecule

$$\sigma_R = \frac{32\pi}{3}\left(\frac{\omega}{c}\right)^4 \frac{\alpha^2}{|1-\Gamma|^2}\left|1+\frac{(1-\epsilon)\xi_0 Q_1'(\xi_1)}{\epsilon Q_1(\xi)-\xi_0 Q_1'(\xi_0)}\right|^4 ; \tag{4.4}$$

This term is proportional to the square of the molecular polarizability; finally, σ_{RM} is a cross term between Rayleigh and Mie scattering

$$\sigma_{RM} = \frac{32\pi}{9}\left(\frac{\omega}{c}\right)^4 \alpha f^3\xi_0 \mathrm{Re}\left[\frac{(\epsilon^*-1)}{(1-\Gamma)[\epsilon^* Q_1(\xi_0)-\xi_0 Q_1'(\xi_0)]} \times\left(1+\frac{(1-\epsilon)\xi_0 Q_1'(\xi_1)}{\epsilon Q_1(\xi_0)-\xi_0 Q_1'(\xi_0)}\right)^2\right] . \tag{4.5}$$

In order to obtain the molecular Raman scattering cross section we must consider inelastic light scattering. We obtain the Raman cross section in a semiclassical manner as discussed in the introduction. We take

$$\alpha = \alpha_0 + \Delta Q\frac{\partial\alpha}{\partial Q}\cos\Omega t , \tag{4.6}$$

where ΔQ is a molecular normal mode coordinate and Ω is the corresponding vibration frequency. In our simplified geometry we neglect variations of the polarizability tensor perpendicular to the axis of symmetry. If we insert Eq. (4.6) in the evaluation of Eq. (4.2), we find that only the Rayleigh term gives rise to a Raman contribution, resulting in

$$\sigma_{RS} = \frac{8\pi}{3}\left(\frac{\omega}{c}\right)^4 (\Delta Q)^2\left(\frac{\partial\alpha}{\partial Q}\right)^2\frac{1}{|1-\Gamma|^4} \times\left|1+\frac{(1-\epsilon)\xi_0 Q_1'(\xi_1)}{\epsilon Q_1(\xi_0)-\xi_0 Q_1'(\xi_0)}\right|^4 . \tag{4.7}$$

In deriving Eq. (4.7) from Eq. (4.3), we have neglected any possible contribution to Raman scattering from $\partial F/\partial Q$.

A second type of Raman process arises from the molecule–metal bond itself. Here we may regard α as constant and assume ξ_1 to be oscillating at the bond frequency Ω',

$$\xi_1 = \xi_1^{(0)} + \frac{\partial\xi_1}{\partial H}\Delta H\cos\Omega' t , \tag{4.8}$$

where ΔH is the transition moment for the metal–molecule bond. Insertion of this expression into the Rayleigh scattering yields

$$\sigma_{RS}' = \frac{8\pi}{3}\left(\frac{\omega}{c}\right)^4\left(\frac{\alpha\Delta H}{f}\right)^2\left|\frac{\xi_0 Q_1''(\xi_1^{(0)})}{1-\Gamma}\right|^2\left|\frac{1-\epsilon}{\epsilon Q_1(\xi_0)-\xi_0 Q_1'(\xi_0)}\right|^2 . \tag{4.9}$$

The expressions given by Eqs. (4.7) and (4.9) are applicable to the case of weak chemisorption or physiosorption. For strong chemisorption the normal mode frequencies will be altered and the coordinates may be expressed in terms of Q_i and H. The separation into two independent expressions, as above, is not possible.

In the limit of a perfect conductor, where $|\epsilon|\to\infty$, these expressions reduce to

$$\sigma_M \to \frac{8\pi}{27}\left(\frac{\omega}{c}\right)^4 f^6\xi_0^2\left(\frac{1}{Q_1^2(\xi_0)}+\frac{4F^2}{[Q_1(\xi_0)+(\xi_0^2-1)^{-1}]^2}\right) , \tag{4.3'}$$

$$\sigma_R \to \frac{32\pi}{3}\left(\frac{\omega}{c}\right)^4\frac{\alpha^2}{|1-\Gamma|^2}\left|1-\frac{\xi_0 Q_1'(\xi_1)}{Q_1(\xi_0)}\right|^4 , \tag{4.4'}$$

$$\sigma_{RM} \to \frac{32\pi}{9}\left(\frac{\omega}{c}\right)^4\frac{\alpha f^3\xi_0}{Q_1(\xi_0)}\frac{1}{1-\Gamma}\left(1-\frac{\xi_0 Q_1'(\xi_1)}{Q_1(\xi_0)}\right)^2 , \tag{4.5'}$$

$$\sigma_{RS} \to \frac{8\pi}{3}\left(\frac{\omega}{c}\right)^4\left(\Delta Q\frac{\partial\alpha}{\partial Q}\right)^2\frac{1}{|1-\Gamma|^4}\left(1-\frac{\xi_0 Q_1'(\xi_1)}{Q_1(\xi_0)}\right)^4 , \tag{4.7'}$$

$$\sigma_{RS}' \to \frac{8\pi}{3}\left(\frac{\omega}{c}\right)^4\left|\frac{\alpha\Delta H}{f(1-\Gamma)}\right|^2\left(\frac{\xi_0 Q_1''(\xi_1)}{Q_1(\xi_0)}\right)^2 . \tag{4.9'}$$

Equations (2.3′), (2.4′), (2.5′), and (2.7′) were obtained earlier.[14] We may further specialize these equations by going to the sphere limit ($\xi_0\to\infty$) and find

$$\sigma_M \to \tfrac{10}{3}\pi(\omega/c)^4 a^6 , \tag{4.3''}$$

which is the familiar Mie scattering cross section formula for a perfectly conducting sphere. In the opposite limit, of a needlelike structure ($\xi_0\to 1$), we have

$$\sigma_M \to \frac{32\pi}{27}\left(\frac{\omega}{c}\right)^4\frac{f^6}{\{\ln[2/(\xi_0-1)]\}^2} , \tag{4.3'''}$$

which shows that Mie scattering gets to be relatively un-

Downloaded 15 Feb 2004 to 132.66.16.12. Redistribution subject to AIP license or copyright, see http://jcp.aip.org/jcp/copyright.jsp

important. The Rayleigh scattering in the sphere limit becomes

$$\sigma_R \to \frac{32\pi}{3}\left(\frac{\omega}{c}\right)^4 \left|\frac{\alpha}{1-\Gamma}\right|^2 \left[1+2\left(\frac{\xi_0}{\xi_1}\right)\right]^4 . \qquad (4.4'')$$

Expressions for the other cross sections in the limiting cases are readily derived.

We define the Raman scattering enhancement factor R as the ratio of Eq. (4.7) to the corresponding expression for an isolated molecule (where $\xi_1 \to \infty$). Then,

$$R = \left| \frac{1+(1-\epsilon)\xi_0 Q_1'(\xi_1)/[\epsilon Q_1(\xi_0) - \xi_0 Q_1'(\xi_0)]}{1-\Gamma} \right|^4 . \qquad (4.10)$$

There are three possibilities for enhancement. The first is when $\Gamma \approx 1$. This is the origin of the enhancement in the so-called image enhancement theories. The second occurs when ξ_0 and ξ_1 are close to unity. This is the enhancement associated with the eccentricity (the "lightning rod" effect) that has been discussed previously.[10] The third corresponds to small $|\epsilon Q_1(\xi_0) - \xi_0 Q_1'(\xi_0)|$ denominators, i.e., to the surface plasmon resonance. On a rough surface the latter two mechanisms are brought into play. This is because differently shaped surface features have differing plasma frequencies and function as more or less effective lightning rods.

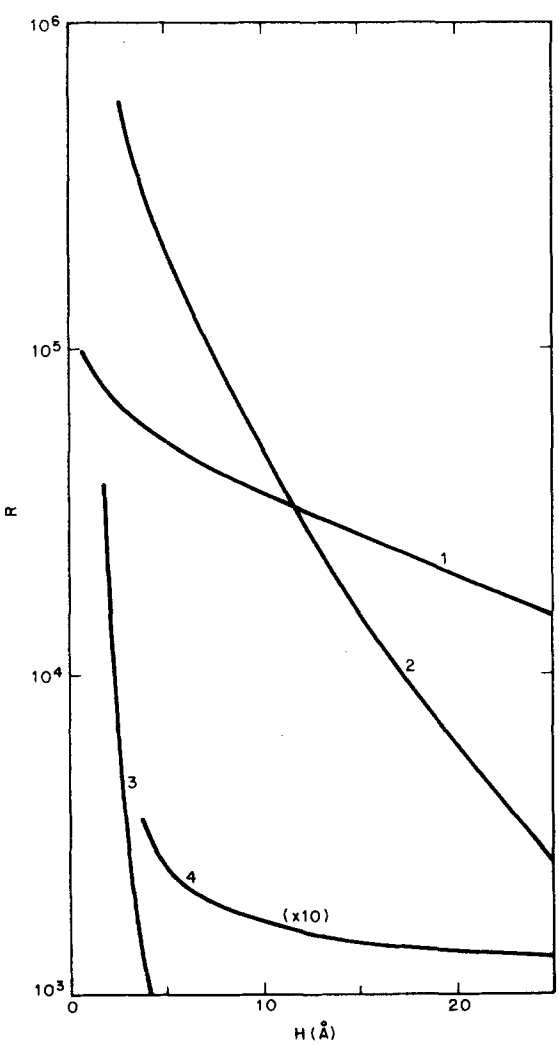

FIG. 3. Enhancement factor R as function of molecule-surface distance H for four sets of (a, b) values: (1) (500, 250) Å; (2) (500, 100) Å; (3) (500, 50) Å; (4) (500, 500) Å. Here $\hbar\omega = 2.50$ eV and $\alpha = 10$ Å^3.

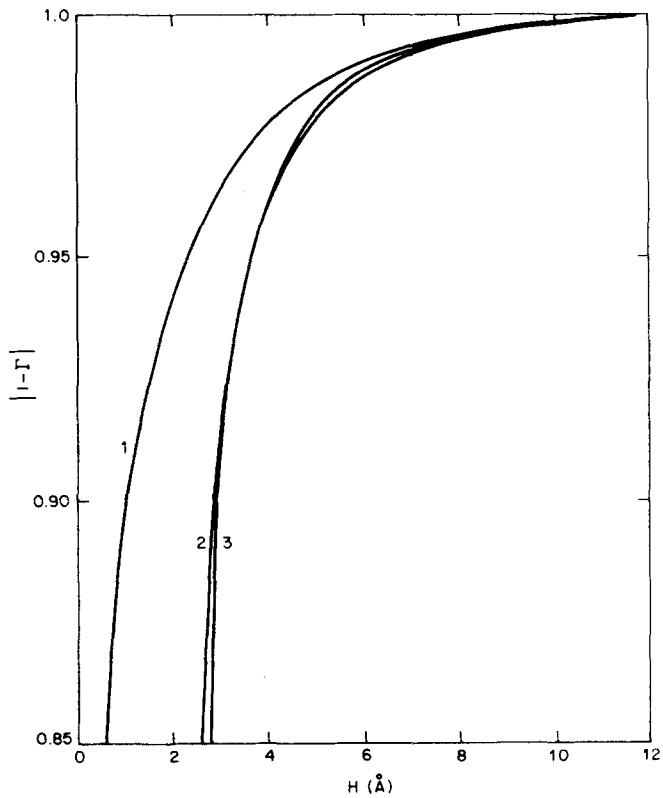

FIG. 4. Magnitude of the image enhancement denominator as a function of H. (1), (2), and (3) denote three surface aspect ratios, as in Fig. 3.

Note that in the present theory the cross section for Raman scattering is proportional to $(\partial\alpha/\partial Q)^2$. If there is, in addition, an electronic resonance of the incident laser with the molecule, a further resonance may ensue. It should be kept in mind, however, that in this case the classical treatment of Raman scattering is no longer valid.

Let us now study the behavior of the enhancement ratio R as a function of the parameters of the theory. In our calculations we take the numerical value of the molecular polarizability to be 1–10 Å^3—typical of small organic molecules. The other length scales in the problem are the semimajor and semiminor axes of the prolate spheroid, a and b, and the distance of the molecule from the surface H. In the figures these will be given in Å. It should be noted, however, that all lengths may be scaled by the same numerical factor (and α by that factor cubed) and the curves will remain valid.

In Fig. 3, we plot the enhancement ratio as a function of distance from the surface for various hemispheroids. The photon energy is taken to be 2.50 eV. The geometry here is a finite hemispheroid on a perfectly conducting plane. We note that enhancement ratios of 10^4–10^6 are possible close to the surface. As one goes away from the surface the enhancement factor declines in a way which depends on the hemispheroid shape. For the less

Downloaded 15 Feb 2004 to 132.66.16.12. Redistribution subject to AIP license or copyright, see http://jcp.aip.org/jcp/copyright.jsp

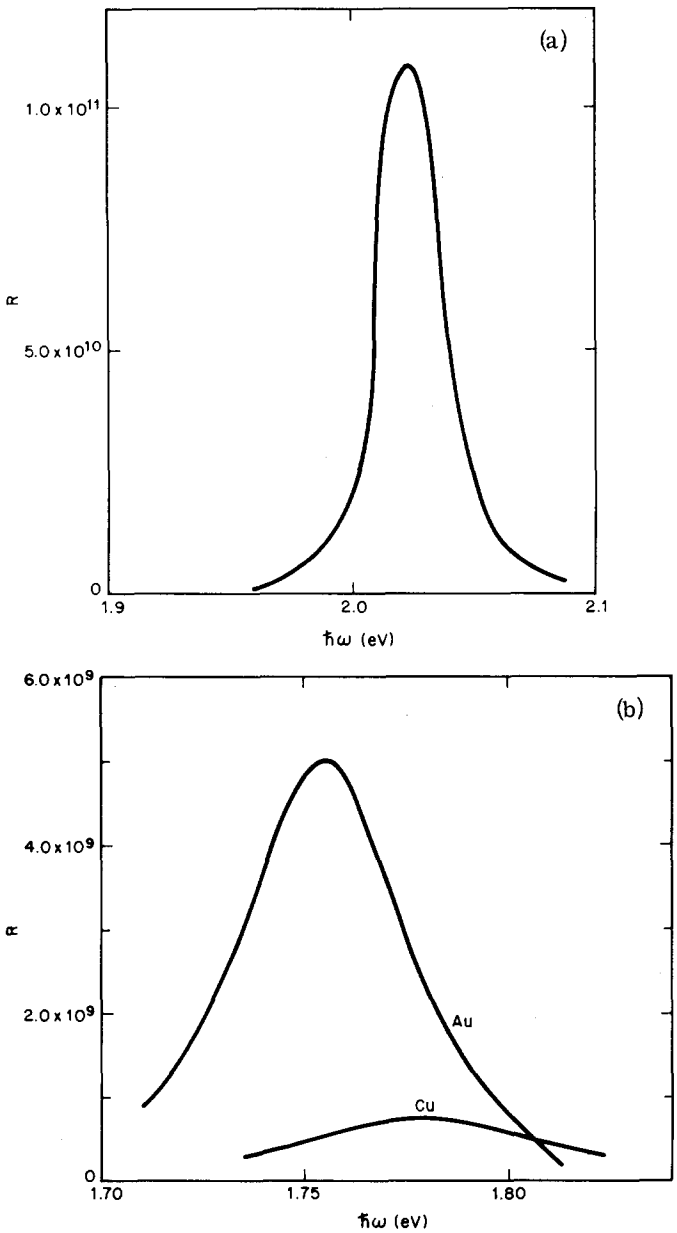

FIG. 5. (a) Enhancement ratio for a molecule adsorbed on Ag vs photon energy in the neighborhood of the surface plasmon resonance. Here $a = 500$ Å, $b = 100$ Å, $H = 5$ Å, and $\alpha = 10$ Å^3. (b) Same as (a) but for Au and Cu.

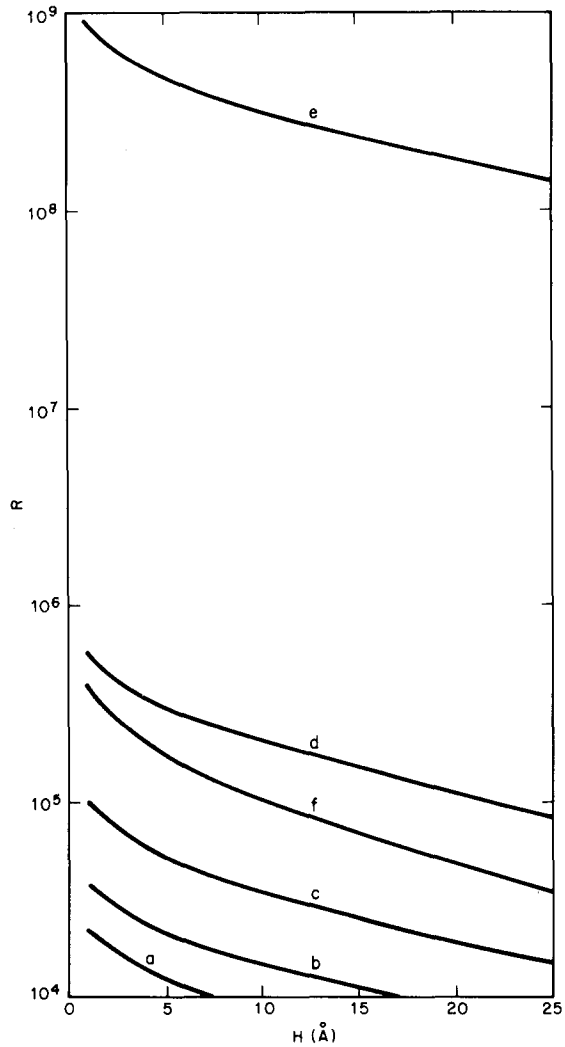

FIG. 6. Enhancement ratio of Ag vs distance from surface for several photon energies. Here $a = 500$ Å, $b = 250$ Å, and $\alpha = 10$ Å^3. Note the fairly slow fall off with distance. The labels (a)–(f) refer to photon energies of 2.01, 2.26, 2.50, 2.75, 3.00, and 3.25 eV, respectively.

eccentric spheroid the fall off is more gradual and appreciable enhancement factors persist out to large distances.

The rapid rise in the enhancement factor at small H is due to the image enhancement effect. This may be seen by plotting (for $\alpha = 10$ Å^3) the magnitude of $1 - \Gamma$ as a function of H in Fig. 4. The value of $|1 - \Gamma|$ is very close to 1 for $H > 4$ Å. For small H, however, Γ grows in magnitude and causes strong enhancement in the region where $\Gamma \approx 1$. The strength of this pole is diluted by the fact that ϵ has an imaginary part. One may also have to consider the finite molecular size and also quantum mechanical corrections to the image effect and to the molecule–surface interaction when the charge cloud of the molecule is close to the surface.

The effect of the surface plasmon resonance is rather pronounced as the photon frequency approaches the (dipolar) surface plasmon. As one may see from Fig. 2, this occurs at $\hbar\omega = 2.02$ eV for Ag with an a to b ratio of 5. In Fig. 5 we plot the enhancement factor as a function of photon energy near this photon energy and see a strong resonant enhancement occurring. Enhancement ratios of 10^{11} are possible for Ag even without the image enhancement mechanism coming in. In Fig. 6 the R factor is plotted as a function of distance H for a number of photon energies. One sees that the effect of the plasmon resonance is to increase the magnitude of the enhancement without affecting its functional behavior with distance.

In Fig. 7 we compare the distance behavior of three different metals Ag, Au, and Cu for fixed geometry and fixed photon energy. The behaviors are seen to be similar, with Ag more effective than Cu which, in turn, is more effective than Au. Of course if the incident radiation resonates with a particular surface plasmon energy then this ordering may be altered.

In Fig. 8 four different cases are compared. Curve

Downloaded 15 Feb 2004 to 132.66.16.12. Redistribution subject to AIP license or copyright, see http://jcp.aip.org/jcp/copyright.jsp

(a) is for a perfectly conducting hemispheroidal protrusion on a perfectly conducting plane. Curve (b) is for an isolated perfectly conducting spheroid and curve (c) is for an isolated spheroid with a realistic $\epsilon(\omega)$ for Ag. Curve (d) is for the model of a Ag hemispheroid on a conducting plane. One sees that the curves are all similar but that factors of one order of magnitude may arise from case to case.

In the immediate vicinity of a solid state surface one expects a variation of the intrinsic surface electrostatic potential from point to point in a direction parallel to the surface. This is consistent with the existence of different work functions for different faces of the same metal. If the surface is rough, one would expect the strongest intrinsic electric fields near the sharpest protrusions. If molecules are deposited on a surface they migrate towards the lowest energy sites. The states of lowest physisorption energy are precisely these protrusions. In the case of a polarizable object, the polarization energy is $U = -\frac{1}{2}\alpha E^2$. For a dipole μ one has a minimum energy $U' = -\mu E$, etc. Thus the first molecules to be deposited are likely to cover the sharp protrusions. However, we have seen that these sharp features are precisely the ones which have the largest Raman enhancement factor.

A simple conclusion may be drawn from this observation. If one were to increase the adsorbate coverage from zero to some finite value one would expect to see a very rapid rise in the SERS signal at submonolayer coverages. This signal should then rise more slowly as the rest of the surface is covered. This is consistent with recent data of the Bell group[6] and is evidence that only a small part of the surface is active in SERS.

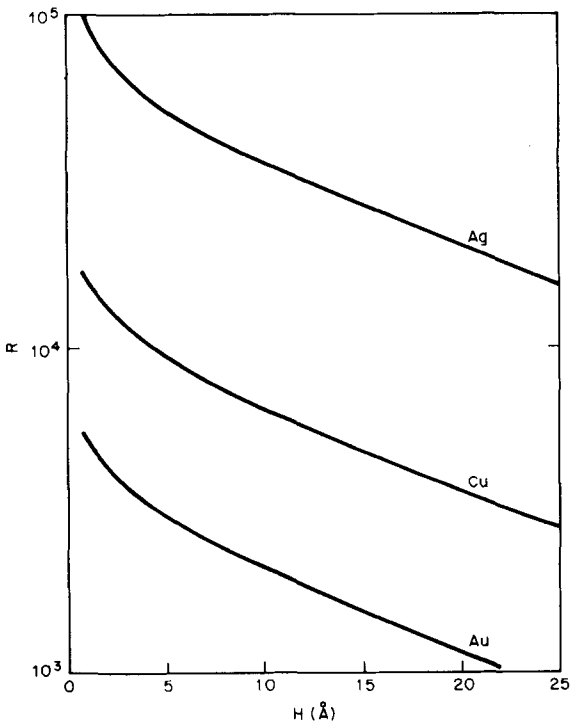

FIG. 7. Enhancement ratio of Ag, Cu, and Au as a function of molecule–metal distance. Here $a = 500$ Å, $b = 250$ Å, $\hbar\omega = 2.50$ eV, and $\alpha = 10$ Å^3.

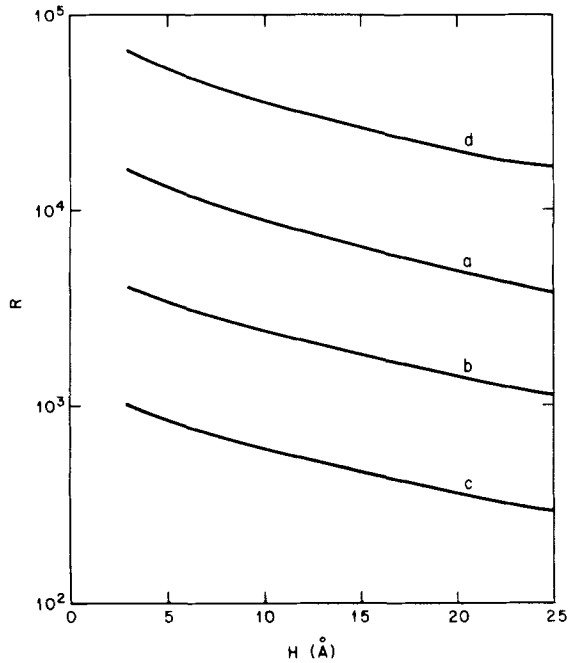

FIG. 8. Enhancement ratio as a function of molecule–metal distance for four cases: (a) isolated silver spheroid with $a = 500$ Å and $b = 250$ Å; (b) perfectly conducting hemispheroid of the same size on a conducting plane; (c) isolated perfectly conducting spheroid of the same size; (d) silver hemispheroid on a conducting plane. Here $\hbar\omega = 2.50$ eV and $\alpha = 10$ Å^3.

In our analysis we have seen that as the aspect ratio increases a fall off of the SERS signal at large distances from the surface occurs (see Fig. 3). However, sharp aspect ratios are correlated with low photon energies due to the surface plasmon resonance (see Fig. 2). Thus one expects to see a diminution of the long range property of SERS as one goes to longer wave lengths of the exciting light.

The results obtained so far correspond to a rather restricted geometry: the molecule lies on the symmetry axis, the external field and the induced molecular dipole are parallel to this axis. In the following section we consider the effect of the dipole orientation relative to the surface and obtain the complete effective Raman polarizability tensor for the particular case of a molecule adsorbed on a sphere.

V. POLARIZABILITY AND RAMAN SCATTERING OF A MOLECULE ADSORBED ON A METAL SPHERE: GENERAL STRUCTURE AND ORIENTATION

In Secs. II–IV we have analyzed light scattering in general and Raman scattering in particular resulting from a field incident on a molecule–hemispheroid system in the configuration shown in Fig. 1. In this section we investigate the directionality and polarization properties of the Raman scattering by allowing the molecular dipole to assume a general orientation (defined by the angle θ, Fig. 9) relative to the sphere and by allowing the incident field to be in any given direction and with any given polarization. On the other hand we restrict ourselves to the case of a molecule adsorbed on a perfect sphere. Again the long wavelength limit is

Downloaded 15 Feb 2004 to 132.66.16.12. Redistribution subject to AIP license or copyright, see http://jcp.aip.org/jcp/copyright.jsp

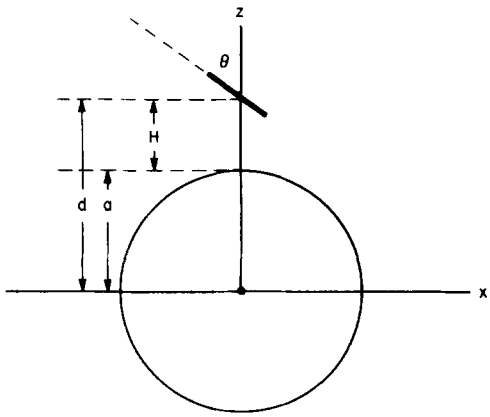

FIG. 9. Molecule–sphere system discussed in Sec. V. The sphere center is the origin; the molecule lies on the z axis and the induced molecular dipole is taken to be in the xz plane.

considered so that the equations of electrostatics may be used. As before, we assume that the Raman polarizability tensor $\Delta Q(\partial\alpha_1/\partial Q)$ is proportional (or parallel) to the molecular polarizability tensor α_1 (the molecular polarizability is now denoted by α_1, to distinguish it from the sphere polarizability). This is always true for a diatomic molecule and also holds for each bond polarizability in a model which represents the molecule as a sum of polarizable bond dipoles. [15]

A complete solution for the effective polarizability of this system may be obtained by solving the Laplace equation in the presence of a homogeneous electric field $\mathbf{E}_0$ in much the same way as described in Sec. II. The potential Φ_I outside the sphere is written as a sum of terms

$$\Phi_I = -\mathbf{E}_0 \cdot \mathbf{r} + \Phi^I_{dip} + \Phi^I_{sph} , \tag{5.1}$$

corresponding to the external field and to the fields associated with the polarizations induced on the molecule (induced dipole in our model) and on the sphere. These terms may be expanded

$$-\mathbf{E}_0 \cdot \mathbf{r} = -\left(\frac{4\pi}{3}\right)^{1/2} r\left(E_{0_z} Y_{1,0}(\theta,\phi) + \frac{E_{0_x} + iE_{0_y}}{\sqrt{2}} Y_{1,-1}(\theta,\phi) - \frac{E_{0_x} - iE_{0_y}}{\sqrt{2}} Y_{1,1}(\theta,\phi)\right) \tag{5.2}$$

$$\Phi^I_{sph} = \sum_{l=0}^{\infty} \sum_{m=-l}^{l} B_{lm} r^{-l-1} Y_{lm}(\theta,\phi) , \tag{5.3}$$

$$\Phi^I_{dip} = -\frac{\mu_1}{R_2}\left[\frac{\sin\theta_1}{2} \sum_{l=1}^{\infty} \left(\frac{4\pi l(l+1)}{2l+1}\right)^{1/2} l\left(\frac{r}{d}\right)^l \times [Y_{l,1}(\theta,\phi) + Y_{l,-1}(\theta,\phi)] + \cos\theta_1 \sum_{l=0}^{\infty} \left(\frac{4\pi}{2l+1}\right)^{1/2} (l+1)\left(\frac{r}{d}\right)^l Y_{l,0}(\theta,\phi)\right] \quad (r<d) . \tag{5.4}$$

In particular, in Eq. (5.4), μ_1 is the (induced) molecular dipole. The potential is obtained by an expansion of the expression for the dipole potential in the appropriate set of spherical harmonics. Expanding also the potential inside the sphere in spherical harmoncs

$$\Phi^{II}_{sph} = \sum_{l=0}^{\infty} \sum_{m=-l}^{l} A_{lm} r^l Y_{lm}(\theta,\phi) , \tag{5.5}$$

and applying the usual boundary conditions on the surface of the sphere leads to explicit results for the coefficients A_{lm} and B_{lm} as functions of $\mathbf{E}_0$ and μ_1. Finally adding the equation

$$\mu_1 = \alpha_1 \cdot (\mathbf{E}_0 - \nabla\Phi^I_{sph}) , \tag{5.6}$$

leads to a self-consistent set of equations equivalent to (1.2). From this an expression for μ_1 as a function of $\mathbf{E}_0$ is obtained which yields an expression for the effective molecular polarizability α_1^{eff}. In addition the far field associated with Φ^I_{sph}, Eq. (5.3) is related to the dipole scattering by the sphere and yields an expression for α_1^{eff}. α_1^{eff} and α_2^{eff} are summed to yield the total polarizability.

In order to shed more light on the physical interpretation of the different terms appearing in the final result we derive it in a somewhat different route. Write

$$\mu_1 = \alpha_1 \cdot (\mathbf{E}_0 + \mathbf{E}_{sph}) , \tag{5.7}$$

where $\mathbf{E}_{sph}$ is the field associated with the polarized metal sphere calculated at the position of the molecule. $\mathbf{E}_{sph}$ may in turn be represented as a sum

$$\mathbf{E}_{sph} = \mathbf{E}^{(1)}_{sph} + \mathbf{E}^{(2)}_{sph} , \tag{5.8}$$

where $\mathbf{E}^{(1)}_{sph}$ is associated with the polarization of the sphere by the external field $\mathbf{E}_0$, while $\mathbf{E}^{(2)}_{sph}$ corresponds to the polarization induced by the molecular dipole. Finally a contribution to the Raman scattering comes also from dipolar part of the sphere polarization associated with $\mathbf{E}^{(2)}_{sph}$. In what follows we calculate each component separately.

(a) $\mathbf{E}^{(1)}_{sph}$ is the field of the dipole induced by the external field due to the sphere polarizability $\alpha_2 = a^3(\epsilon-1)/(\epsilon+2)$. It is given by (at the position d of the molecule)

$$\mathbf{E}^{(1)}_{sph} = \mathbf{M}(d)[(\epsilon-1)/(\epsilon+2)]a^3\mathbf{E}_0 , \tag{5.9}$$

where $\mathbf{M}(d)$ is defined by Eq. (1.3).

(b) $\mathbf{E}^{(2)}_{sph}$ is the field, at the location of the molecule resulting from the part of the polarization of the sphere related to the molecular image. We assume that the sphere is large relative to the molecule–sphere distance $H = d - a$. In this case $\mathbf{E}^{(2)}_{sph}$ may be taken as the molecular image field associated with a plane surface

$$\mathbf{E}^{(2)}_{sph} = \frac{\epsilon-1}{\epsilon+1} \mathbf{M}(2d) \cdot \begin{bmatrix} -1 & 0 & 0 \\ 0 & -1 & 0 \\ 0 & 0 & +1 \end{bmatrix} \cdot \mu_1 . \tag{5.10}$$

(c) The far field of the sphere in the presence of the external field $\mathbf{E}_0$ and of the molecular dipole μ_1 may be shown to be that associated with a dipole μ_{sph} given by

$$\mu_{sph} = \frac{\epsilon-1}{\epsilon+2} a^3\mathbf{E}_0 + 2\frac{\epsilon-1}{\epsilon+2}\left(\frac{a}{d}\right)^3 \mu_1^{\perp} - \frac{\epsilon-1}{\epsilon+2}\left(\frac{a}{d}\right)^3 \mu_1^{\parallel} , \tag{5.11}$$

where $\mu_1^{\perp}$ and $\mu_1^{\parallel}$ are, respectively, the normal and parallel (to the sphere surface) components of the molecular dipole. Obviously only the terms associated with μ_1, contribute to the Raman scattering. Their sum $\mu^{(2)}_{sph}$ is

Downloaded 15 Feb 2004 to 132.66.16.12. Redistribution subject to AIP license or copyright, see http://jcp.aip.org/jcp/copyright.jsp

$$\mu_{\rm sph}^{(2)}=\frac{\epsilon-1}{\epsilon+2}\left(\frac{a}{d}\right)^3\begin{bmatrix}-1&0&0\\0&-1&0\\0&0&2\end{bmatrix}\cdot\mu_1\,. \tag{5.12}$$

Inserting Eqs. (5.8), (5.9), and (5.10) into Eq. (5.7) leads to an equation for μ_1 which upon solution yields [using Eq. (5.12)] $\mu_{\rm sph}^{(2)}$. The total Raman scattering is associated with $\mu_1+\mu_{\rm sph}^{(2)}$. Finally, the Raman polarizability is obtained by considering the derivative of the total polarizability with respect to the molecular nuclear coordinate. In executing this procedure we take the bare molecular polarizability to be

$$\alpha_1=\alpha_1\mathbf{U}\,, \tag{5.13a}$$

$$\mathbf{U}=\begin{bmatrix}\sin^2\theta&0&\sin\theta\cos\theta\\0&0&0\\\sin\theta\cos\theta&0&\cos^2\theta\end{bmatrix}\,, \tag{5.13b}$$

such that the induced molecular dipole is in the desired direction (corresponding, e.g., to the relevant molecular bond. Note that the form of Eq. (1.13) imply that α_1 and $\partial\alpha_1/\partial Q$ are proportional to each other). The result for the total Raman polarizability of the system is found to be

$$\alpha_{\rm RAM}^{\rm tot}=\Delta Q\,\frac{\partial\alpha_1}{\partial Q}\,(\mathbf{I}+\mathbf{M}(d)\cdot\alpha_2)\cdot(\mathbf{I}-\mathbf{\Gamma}_p)^{-2}\cdot\mathbf{U}\cdot(\mathbf{I}+\mathbf{M}(d)\cdot\alpha_2)\,, \tag{5.14}$$

where

$$\mathbf{\Gamma}_p=\alpha_1\mathbf{U}\cdot\mathbf{M}\,(2d)\begin{bmatrix}-1&0&0\\0&-1&0\\0&0&1\end{bmatrix}\frac{\epsilon-1}{\epsilon+1}\,, \tag{5.15}$$

$$\alpha_2=[(\epsilon-1)/(\epsilon+2)]a^3\mathbf{I}\,, \tag{5.16}$$

and where ($\hat{n}$ being a unit vector in the z direction)

$$\mathbf{M}(d)=\frac{3\hat{n}\hat{n}-1}{d^3}=\frac{1}{d^3}\begin{bmatrix}-1&0&0\\0&-1&0\\0&0&2\end{bmatrix}\,. \tag{5.17}$$

Equation (5.14) provides a good approximation to the total Raman polarizability of the molecule–sphere system if all the spatial dimensions of this sytem are much smaller than the radiation wavelength and if the sphere radius is much larger than the molecule–sphere separation. A useful approximation to Eq. (5.14) is obtained by neglecting the image terms involving $(\mathbf{I}-\alpha_1\mathbf{\Gamma}_p)^{-1}$. Using Eq. (5.15) and the fact that α_1 is usually of the order of atomic volumes, it is seen that this approximation is valid at molecule–sphere distance > 4 Å. It leads to

$$\alpha_{\rm RAM}^{\rm tot}=(\mathbf{I}+\mathbf{M}(d)\cdot\alpha_2)\mathbf{U}(\mathbf{I}+\mathbf{M}(d)\cdot\alpha_2)\,\frac{\partial\alpha_1}{\partial Q}\,\Delta Q\,. \tag{5.18}$$

Using the expressions for $\mathbf{M}$, α_2, and $\mathbf{U}$ given above, this leads to the explicit result

$$\alpha_{\rm RAM}^{\rm tot}=\Delta Q\,\frac{\partial\alpha_1}{\partial Q}\begin{bmatrix}(1-\beta)^2\sin^2\theta&0&(1-\beta)(1+2\beta)\sin\theta\cos\theta\\0&0&0\\(1-\beta)(1+2\beta)\sin\theta\cos\theta&0&(1+2\beta)^2\cos^2\theta\end{bmatrix}\,, \tag{5.19}$$

where

$$\beta=[(\epsilon-1)/(\epsilon+2)]\,(a/d)^3\,. \tag{5.20}$$

$\alpha_{\rm RAM}^{\rm tot}$ from Eq. (5.14) or (5.15) can now be used to calculate the Raman scattering cross section for any given excitation–detection configuration. The dependence on the structure of the molecule–sphere complex is expressed by the parameters d, a, and the angle θ). Further averaging may be needed to account for all possible orientations of the molecule–sphere complex relative to the direction of the incident radiation. A complete spherical average is needed, e.g., for evaluating the Raman scattering by molecules adsorbed on colloid particles[16] obtained as follows:

Denote

$$A_R=\mathrm{Re}(1-\beta)^2\,,\quad A_I=\mathrm{Im}(1-\beta)^2\,, \tag{5.21a}$$

$$D_R=\mathrm{Re}(1+2\beta)^2\,,\quad D_I=\mathrm{Im}(1+2\beta)^2\,, \tag{5.21b}$$

$$C_R=\mathrm{Re}[(1-\beta)(1+2\beta)]\,,\quad C_I=\mathrm{Im}[(1-\beta)(1+2\beta)]\,; \tag{5.21c}$$

$\alpha_{\rm RAM}^{\rm tot}$ is the sum of real and imaginary parts

$$\alpha_{\rm RAM}^{\rm tot}=\Delta Q\,\frac{\partial\alpha_1}{\partial Q}\begin{bmatrix}(A_R+iA_I)\sin^2\theta&0&(C_R+iC_I)\sin\theta\cos\theta\\0&0&0\\(C_R+iC_I)\sin\theta\cos\theta&0&(D_R+iD_I)\cos^2\theta\end{bmatrix}\,. \tag{5.22}$$

The rotational invariants

$$\gamma_0=\tfrac{1}{3}\,\mathrm{Tr}\alpha \tag{5.23}$$

and

$$\gamma_1^2=\tfrac{1}{2}[(\alpha_{xx}-\alpha_{yy})^2+(\alpha_{yy}-\alpha_{zz})^2+(\alpha_{zz}-\alpha_{xx})^2+\tfrac{3}{2}[(\alpha_{xy}+\alpha_{yx})^2+(\alpha_{yz}+\alpha_{zy})^2+(\alpha_{zx}+\alpha_{xz})^2]\}\,, \tag{5.24}$$

$$\gamma_2^2=\tfrac{3}{4}[(\alpha_{xy}-\alpha_{yx})^2+(\alpha_{yz}-\alpha_{zy})^2+(\alpha_{zx}-\alpha_{xz})^2]\,, \tag{5.25}$$

Downloaded 15 Feb 2004 to 132.66.16.12. Redistribution subject to AIP license or copyright, see http://jcp.aip.org/jcp/copyright.jsp

are obtained separately for the real and the imaginary parts. We get

$$\gamma_{0R} = \tfrac{1}{3}(A_R \sin^2\theta + D_R \cos^2\theta) ,$$
$$\gamma_{1R}^2 = A_R^2 \sin^4\theta + D_R^2 \cos^4\theta + \tfrac{1}{4}(3C_R^2 - A_R D_R)\sin^2 2\theta , \quad (5.26)$$
$$\gamma_{2R}^2 = 0 ,$$

with similar expressions for γ_{0I}, γ_{1I}^2, and $\gamma_{2I}=0$, where A_I, C_I, and D_I replace A_R, C_R, and D_R. All rotationally averaged cross sections are obtained in terms of these invariants. We shall calculate for example the scattering cross section corresponding to a nonpolarized incident beam in the $\hat{z}$ direction and a detector lying in the $\hat{x}$ direction which sums over all final polarizations. Equation (1.9) leads to the following expression for the relevant cross section:

$$\frac{d\sigma}{d\Omega} = \frac{k^4}{2}\left[\left|(\alpha_{\mathrm{RAM}})_{yx}\right|^2 + \left|(\alpha_{\mathrm{RAM}})_{yy}\right|^2 + \left|(\alpha_{\mathrm{RAM}})_{zx}\right|^2 + \left|(\alpha_{\mathrm{RAM}})_{zy}\right|^2\right] , \quad (5.27a)$$

which on rotational averaging yields

$$\left\langle\frac{d\sigma}{d\Omega}\right\rangle = \frac{k^4}{2}\left|\Delta Q\,\frac{\partial\alpha_1}{\partial Q}\right|^2 (\gamma_{0R}^2 + \gamma_{0I}^2 + \tfrac{13}{45}(\gamma_{1R}^2 + \gamma_{1I}^2)) . \quad (5.27b)$$

To obtain this result we have used

$$\langle\alpha_{xy}^2\rangle = \langle\alpha_{yz}^2\rangle = \langle\alpha_{zy}^2\rangle = \tfrac{1}{15}\gamma_1^2 + \tfrac{1}{9}\gamma_2^2 ,$$
$$\langle\alpha_{yy}^2\rangle = \gamma_0^2 + \tfrac{4}{45}\gamma_1^2 . \quad (5.28)$$

[cf. Ref. 17, Eqs. (3.23), (3.24), and (5.59)]. $\langle\,\rangle$ denotes rotational averaging and γ_0, γ_1 are the rotational invariants of the tensor α. Finally, we note that the free molecule limit is obtained by taking $\epsilon = 1$, when $\beta = 0$. Then

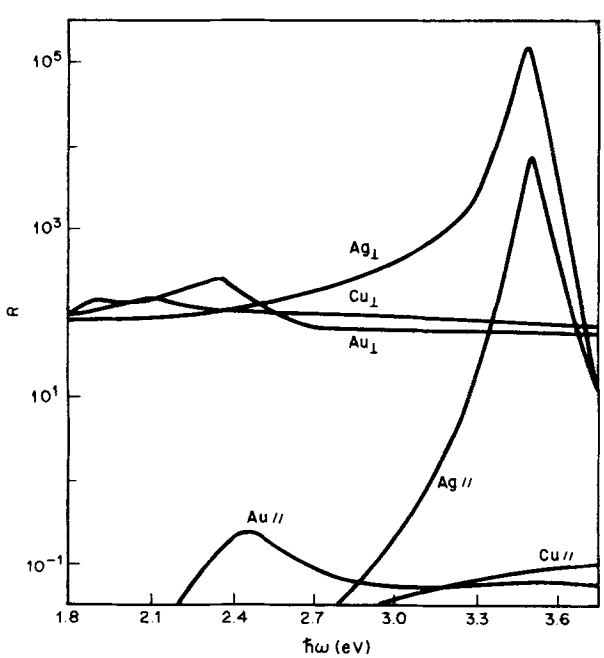

FIG. 10. Raman enhancement ratios for a molecule adsorbed on silver, copper, and gold spheres. The induced is perpendicular (⊥) or parallel (∥) to the metal surface. Parameters used: $a = 100$ Å, $d = 5$ Å, and $\alpha_1 = 1.0$ Å^3.

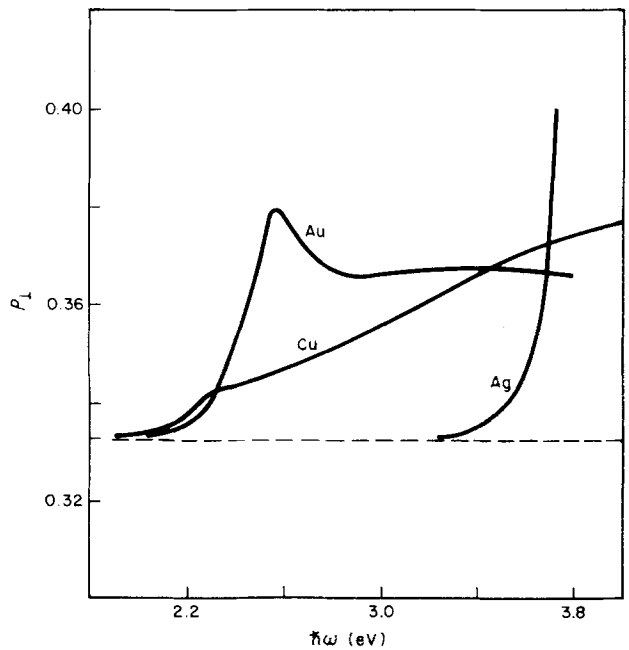

FIG. 11. Raman enhancement ratios for a molecule adsorbed on Ag, Cu, and Au spheres as a function of the bond orientation θ. (a) Ag with incident photon energy 3.5 eV; (b) Ag (2.5 eV); (c) Cu (2.13 eV); (d) Au (2.34 eV). The energies 3.5, 2.13, and 2.34 eV correspond to maximum enhancement ratios for Ag, Cu, and Au, respectively, in the normal (⊥) orientation (Fig. 10).

$A_R = C_R = D_R = 1$ and $A_I = C_I = D_I = 0$. This implies $\gamma_{0I} = \gamma_{1I} = 0$ and $(\gamma_0)_{\mathrm{free}} = \frac{1}{3}$, $(\gamma_1)_{\mathrm{free}} = 1$,

$$\left(\frac{d\sigma}{d\Omega}\right)_{\mathrm{free}} = \frac{k^4}{2}\,\frac{2}{5}\left|\Delta Q\,\frac{\partial\alpha_1}{\partial Q}\right|^2 . \quad (5.29)$$

The enhancement factor is

$$R = \tfrac{5}{2}[\gamma_{0R}^2 + \gamma_{0I}^2 + \tfrac{13}{45}(\gamma_{1R}^2 + \gamma_{1I}^2)] . \quad (5.30)$$

For the tangential configuration (molecular dipole parallel to sphere surface) $\theta = \frac{1}{2}\pi$, $\gamma_0 = \frac{1}{3}A$, $\gamma_1 = A$. In the normal configuration (molecular) dipole perpendicular to the sphere surface), $\theta = 0$, $\gamma_0 = \frac{1}{3}D$, $\gamma_1 = D$. Inserting into Eq. (5.30), we get

$$R_t = A_R^2 + A_I^2 = |1-\beta|^4 , \quad (5.31a)$$
$$R_t = D_R^2 + D_I^2 = |1+2\beta|^4 . \quad (5.31b)$$

R_t and R_n are the enhancement factors for the tangential and normal configurations, respectively. Considerable enhancement is expected when $|\beta| \gg 1$, i.e., when the incident frequency is such that $|[\epsilon(\omega)-1]/[\epsilon(\omega)+2]| \gg 1$, i.e., near the surface plasmon (dipole) resonance of the metal sphere corresponding to frequency range for which $|\epsilon(\omega)+2| \sim 0$.

The same procedure for rotational averaging may obviously be carried for the more accurate expression Eq. (5.14) which contains also the image effect. This more general expression has been used to obtain the results displayed in Fig. 10. A comparison of Raman enhancement factors R_t and R_n for silver, copper, and gold is shown in Fig. 10, while the dependence of the maximum enhancement factors for the three metals on the molecular orientation is displayed in Fig. 11. In general the

Downloaded 15 Feb 2004 to 132.66.16.12. Redistribution subject to AIP license or copyright, see http://jcp.aip.org/jcp/copyright.jsp

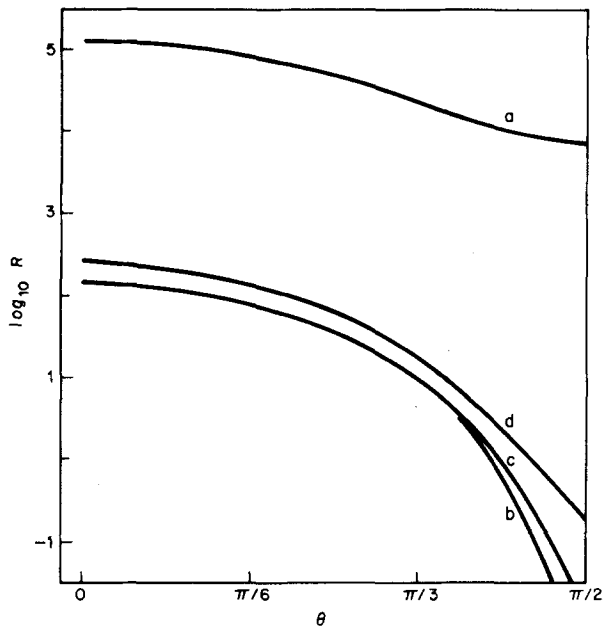

FIG. 12. Depolarization ratios for Raman scattering of a molecule–metal sphere system with rotational averaging. For normal detection geometry and for incident field perpendicular to the scattering plane. Energy dependent depolarization ratios are obtained for $\theta \neq 0$, $\frac{1}{2}\pi$ ($\theta = \frac{1}{4}\pi$ in figure) while the ratio is $\frac{1}{3}$ independent of metal and energy for the perpendicular ($\theta = 0$) and tangential ($\theta = \frac{1}{2}\pi$) configurations.

normal configuration ($\theta = 0$) is the most effective in the Raman scattering process, while for the tangential configuration Raman scattering is very weak (except in cases of very strong enhancement). This result may be traced to the destructive (in the tangential case) interference between the radiation originating in the molecular dipole and between that originating in its image.

Finally, given the complete Raman polarizability tensor we may also calculate depolarization ratios for the radition scattered from different configurations. For a complete spherical average the depolarization ratio associated with incident electric field perpendicular to the scattering plane and detection normal to the direction of the incident radiation is given by [Ref. 17, Eq. (5.61)]

$$\rho_{\perp}(\tfrac{1}{2}\pi) = (3\gamma_1^2 + 5\gamma_2^2)/(45\gamma_0^2 + 4\gamma_1^2) \,. \tag{5.32}$$

This quantity is shown as a function of incident frequency for silver, copper, and gold in Fig. 12. Such measurements can, in principle, determine the structure of the molecule–metal particle complex.

VI. CONCLUSIONS

We have identified three major electromagnetic contributions to the Raman scattering enhancement ratio: (a) the image enhancement mechanism, (b) the lightning rod effect, and (c) the resonance with the surface plasmon associated with the eccentric surface feature. The image mechanism may be operative at close range ($H < 4$ Å), however its true nature has to be investigated with the quantum mechanical nature of the surface, the molecule and their interaction taken into account. It is interesting to note that if the image mechanism is disregarded, the resulting Raman cross-section of the molecule–surface irregularity system is proportional to that of the free molecule, in general agreement with experimental observations. The lightning rod and the surface plasmon resonance effects contribute in two ways: first by increasing the electric field seen by the molecule, thereby increasing the apparent scattering cross-section, and secondly by affecting the polarization of the metal by the molecular dipole which constitutes an additional source of Raman intensity. In addition we have studied the effect of the structure of the molecule–metal particle complex on the enhancement and on the directional and polarization properties of the scattered light.

The enhancement ratio was shown to be strongly dependent on the shape of the metal protrusion both through the effectiveness of the lightning rod mechanism and through the shape dependence of the surface plasmon resonance frequency. We have seen that for favorable cases of protrusion shape and adsorption geometry the enhancements mechanism may combine to give enhancement ratios of 10^{11} or more. A realistic surface contains many protrusions as well as many flat regions. Only a small fraction of the adsorbed molecules will be located in such "favorable" positions. It may be that while average enhancement ratios of 10^4–10^6 are observed, the dominant effect is produced by this small fraction of the molecules which individually give rise to much larger enhancement.

The shape dependence of the surface plasmon resonance frequency also explains why different, apparently conflicting results are obtained for the frequency dependence of the SERS effect: Differently prepared surfaces are characterized by different distributions of size and shapes of surface irregularities. The observed enhancement ratio and its frequency dependence are obtained by averaging over these distributions and will therefore depend on the nature of the surface.

Our results are in agreement with the recent experimental observations of SERS of pyridine on rough silver surfaces.[6] This study indicates that the presence of relatively large (~1000 Å) silver particles on the surface is necessary for efficient enhancement ($R > 10^2$). Furthermore the mild distance dependence of the enhancement ratio (averaged enhancement of 10^4 is observed up to distances of ~50 Å from the surface[6]) suggest that particles of aspect ratios in the range 1–2 play the most important role (see Fig. 3).

The main shortcoming of the present treatment is that it disregards the interaction between the metal protrusions and metal particles lying on the surface. This interaction gives rise to collective electron resonances which were discussed in connection with SERS by Moscovits[8] and by Burstein, Chen, and Lundquist.[9] Collective resonances are shifted relative to the corresponding single particle resonance and their presence will affect the present results. We also note the other simplifying features taken in the present calculation: the underlying planar surface was taken to be a perfect

Downloaded 15 Feb 2004 to 132.66.16.12. Redistribution subject to AIP license or copyright, see http://jcp.aip.org/jcp/copyright.jsp

conductor and the surface protrusions were assumed to be much smaller than the wavelength of light. Also we have made a detailed calculation only of the case where the incident electric field is perpendicular to the surface. In this case the problem on a surface is a simple generalization of the isolated spheroid case. A parallel component in the field will induce surface currents in the underlying plane which may modify the light scattering.

Finally the calculation is completely classical; in particular the Raman frequency shift between the incident and scattered radiation which comes naturally in quantum and in semiclassical calculations was disregarded in calculating the enhancement ratio. Because of these reasons our results should be regarded as qualitative. The general agreement of the present theory with the experimental results suggest that the necessary modifications are not very large.

An interesting conclusion of the present study is that the enhanced Raman effect is not inherently a macroscopic–surface phenomenon, but is rather related to the proximity of the molecule to a small metal particle. Enhanced Raman scattering of molecules adsorbed on silver and gold sol particles was indeed observed[16] (the present results are not directly applicable because the long wavelength limit used here is not valid under the reported experimental conditions). Similar effects sho should be observable in matrix ioslated molecule metal particle mixtures and in molecule–metal atoms cluster prepared in a supersonic jet.

Finally we note that the strong local electric field induced by a metal particle at the position of an adsorbed molecules may have other consequences in addition to causing the apparent Raman enhancement. Under favorable conditions the local electric field experienced by the molecule is 10^2–10^3 times stronger than the incident field. This implies that nonlinear optical processes and molecular ionization may occur at incident field intensities much lower than in the isolated molecular case. This interesting possibility deserves further experimental and theoretical study.

ACKNOWLEDGMENTS

One of us (A. N.) would like to thank C. A. Murray for very helpful communication and discussions and L. E. Brus, V. E. Bondybey, H. Metiu, and J. Worlock for helpful discussions. Another of us (J. G.) would like to thank R. Birke, J. L. Birman, R. Lombardi, A. Genack, and D. Weitz for stimulating discussions. The support of the U. S. –Israel Binational Science Foundation, Jerusalem is acknowledged by one of us (A. N.).

[1]M. Fleischman, P. J. Hendra, and A. J. McQuillan, Chem. Phys. Lett. **26**, 123 (1974).
[2]D. L. Jeanmaire and R. P. Van Duyne, J. Electr. Chem. **84**, 1 (1977).
[3]M. G. Albrecht and J. A. Creighton, J. Am. Chem. Soc. **99**, 5215 (1977).
[4]For recent reviews, see (a) R. P. Van Duyne, *Chemical and Biological Applications of Lasers*, edited by C. B. Moore, Vol. 4 (Academic, New York, 1978); (b) E. Burstein, C. Y. Chen, and S. Lundquist, *Proceedings of the Joint US–USSR Symposium on the Theory of Light Scattering Condensed Matter* (Plenum, New York, 1979); (c) S. Efrima and H. Metiu, Israel J. Chem. **17**, 18 (1979); Surf. Sci. **92**, 417 (1980).
[5]T. H. Wood and M. V. Klein, J. Vac. Sci. Technol. **16**, 459 (1979).
[6]J. E. Rowe, C. V. Shank, D. A. Zwemer, and C. A. Murray, Phys. Rev. Lett. **44**, 1770 (1980); D. L. Allara, M. Rhinewine, and C. A. Murray (unpublished).
[7]F. W. King and George C. Schatz, Chem. Phys. **38**, 245 (1979); F. Burstein, Y. J. Chen, C. Y. Chen, S. Lundquist, and E. Tosatti, Solid State Commun. **29**, 565 (1979); A. Otto, Proceedings of the Conference on Vibrations in Adsorbed Layers, Julich, Germany (1978) (unpublished).
[8]M. Moscovits, (a) J. Chem. Phys. **69**, 4159 (1978); and (b) Proceedings of the US–Japan Seminar, in Solid State Commun. **32**, 59 (1979).
[9]E. Burstein, C. Y. Chen, and S. Lundquist, in Refs. 4 and 8(b).
[10]J. Gersten, J. Chem. Phys. (to be published).
[11]F. W. King, R. P. Van Duyne, and G. C. Schatz, J. Chem. Phys. **69**, 4472 (1978).
[12]S. Efrima and H. Metiu, J. Chem. Phys. **70**, 1602 (1979); **70**, 2297 (1979); **70**, 1939 (1979).
[13]P. B. Johnson and R. W. Christy, Phys. Rev. B **6**, 4370 (1972).
[14]J. Gersten, J. Chem. Phys. (to be published).
[15]J. Kirtley, D. J. Scalapino, and P. K. Hansma, Phys. Rev. B **14**, 3177 (1976).
[16]J. A. Creighton, C. G. Blatchford, and M. G. Albrecht, J. Chem. Soc. Faraday Trans. II **75**, 790 (1979).
[17]D. A. Long, *Raman Spectroscopy* (McGraw-Hill, New York, 1977).

Downloaded 15 Feb 2004 to 132.66.16.12. Redistribution subject to AIP license or copyright, see http://jcp.aip.org/jcp/copyright.jsp